Shape coexistence in neutron-deficient Kr isotopes: Constraints on the single-particle spectrum of self-consistent mean-field models from collective excitations

M. Bender,[1,2,3] P. Bonche,[4,*] and P.-H. Heenen[1]

[1]*Service de Physique Nucléaire Théorique, Université Libre de Bruxelles, Case Postale 229, B-1050 Bruxelles, Belgium*

[2]*National Superconducting Cyclotron Laboratory, Michigan State University, East Lansing, Michigan 48824, USA*

[3]*CEA-Saclay DSM/DAPNIA/SPhN, F-91191 Gif-sur-Yvette, France*

[4]*Service de Physique Théorique, CEA Saclay, F-91191 Gif sur Yvette Cedex, France*

(Received 31 May 2006; published 22 August 2006)

We discuss results obtained in the study of shape coexistence in the neutron-deficient $^{72-78}$Kr isotopes. The method that we used is based on the mixing of axial mean-field configurations after their projection on particle number and angular momentum. The calculations are performed with a Skyrme interaction and a density-dependent pairing interaction. Although our calculation reproduces qualitatively and quantitatively many of the global features of these nuclei, such as coexistence of prolate and oblate shapes, their strong mixing at low angular momentum, and the deformation of collective bands, the ordering of our calculated low-lying levels is at variance with experiment. We analyze the role of the single-particle spectrum of the underlying mean field for the spectrum of collective excitations.

DOI: 10.1103/PhysRevC.74.024312 PACS number(s): 21.60.−n, 21.10.Re, 21.10.Ky, 27.50.+e

I. INTRODUCTION

In a mean-field framework [1], the presence of low-lying 0^+ states in the spectrum of an even-even nucleus is usually interpreted as the manifestation of shape coexistence [2]: each of the 0^+ states, including the ground state, corresponds to a mean-field configuration of a different shape. Nuclei around the neutron-deficient Kr and Sr have very early been considered as among the most favorable ones for the presence of shape coexistence. The first studies were performed for ^{72}Kr and a few neighboring odd nuclei with the help of the Nilsson-Strutinsky approach [3]. Detailed calculations have been carried out since then with an improved microscopic-macroscopic model [4] and with self-consistent mean-field models using nonrelativistic Skyrme [5] and Gogny [6] interactions, as well as relativistic Lagrangians [7]. They confirm the presence of oblate and prolate minima in the deformation energy surface of some light Kr, Sr, and Zr isotopes.

The existence of nearly degenerate structures corresponding to different deformations raises immediately the question of their stability against dynamical effects beyond a mean-field approach. One can expect that the physical states result in fact from a mixing of states with spherical, prolate, and oblate deformations. Such mixings were obtained from models with parameters specifically adjusted to the data: the proton-neutron interacting boson model (IBA-2) [8] and a Bohr-Hamiltonian calculation built on a microscopic-macroscopic model [9].

An alternative to a mean-field description of shape coexistence is given by the shell model. However, the number of active particles and holes necessary to describe the neutron-deficient Kr isotopes is prohibitively large, and this mass region is out of reach of the conventional shell model. The problem is tractable in models by performing a clever truncation of the configuration space, as in the complex excited VAMPIR approach using a phenomenologically modified nuclear matter G matrix as residual interaction [10,11] or in the shell-model Monte Carlo (SMMC) method. A SMMC calculation using a schematic pairing + quadrupole interaction is presented in Ref. [12].

The first experimental evidence for ground-state deformation in neutron-deficient Kr isotopes was found in Ref. [13]. Subsequent experiments revealed the rich structure of the low-lying excitation spectrum in these nuclei, with coexisting and mixed bands in $^{72-78}$Kr [14–16]. Much more data on transition probabilities, both in and out of bands, have also now become available [17–27].

The description of such nuclei is a challenge for nuclear structure models. In general, their excitation spectrum varies very rapidly along a given isotopic line. For this reason, they constitute a testing ground for beyond-mean-field approaches built on Skyrme-Hartree-Fock [28,29]. In this paper, we present an application of an angular-momentum-projected generator coordinate method to the description of the low-energy excitations in $^{72-78}$Kr. At present, our implementation of the method is limited to axial mean-field states that are invariant under spatial inversion and time reversal. Applications of the same method to shape coexistence in neutron-deficient Pb isotopes were presented in Refs. [30,31]. A good qualitative agreement with the data was obtained, in particular for the relative position of the coexisting bands that result from a mixing of oblate, spherical, and prolate configurations. However, the mixing is extremely sensitive to many details of the model and to the effective interaction, preventing a detailed quantitative agreement with the data. Compared to the neutron-deficient Pb isotopes, the description of the neutron-deficient Kr isotopes looks simpler. The coexisting bands result from the mixing of only two kinds of structures, oblate and prolate. The number of spherical j shells that contribute to the shell structure is smaller than for Pb, and the shells are the same for neutrons and protons. It is therefore easier to relate the collective states to the underlying mean field.

*Deceased.

Our calculated values presented in the following have already been used for comparison in the experimental report of Refs. [24,25].

II. THE METHOD

The starting point of our method is a set of axial HF + BCS wave functions. They are generated by self-consistent mean-field calculations on a three-dimensional mesh in coordinate space [5,32], with a constraint on a collective coordinate, the axial quadrupole moment $\langle Q_{20}\rangle$. In a spherical nuclear shell model picture, such mean-field states incorporate particle-particle correlations through pairing and many-particle many-hole correlations through nuclear deformation. As a result, the mean-field states break several symmetries of the exact many-body states. These symmetry violations make it difficult to connect mean-field results, expressed in the intrinsic frame of reference of the nucleus, to spectroscopic data, obtained in the laboratory frame of reference. This motivates the second step of our method, the restoration of the symmetries associated with particle numbers and rotation. Another ambiguity in the interpretation of mean-field results arises when the deformation energy varies slowly as a function of a shape degree of freedom, in particular when a potential energy surface presents several minima separated by a low barrier. In such a case, to assign a physical state to each minimum is not a well-founded approximation. This problem is eliminated by the third step of our method: for each angular momentum, states obtained by projecting mean-field configurations of different deformation are used as the generating functions of the generator coordinate method (GCM). The weight coefficients of the mixing are determined by varying the energy and by solving the Hill-Wheeler-Griffin equation [33]. The configuration mixing removes the contribution of vibrational excitations from the ground-state wave function. It also permits construction of a spectrum of excited states. A detailed introduction to the method has been given in Ref [34].

The same effective interaction is used to generate the mean-field states and to perform the configuration mixing: the Skyrme interaction SLy6 [35] in the particle-hole channel and a density-dependent, zero-range interaction in the pairing channel. As required by the SLy6 parametrization, the full two-body center-of-mass correction is included in the variational equations to generate the mean field and in the calculation of the projected GCM energies. The strength of the pairing interaction is the same as in previous studies of light and medium-mass nuclei, that is, -1000 MeV fm^3 for protons and neutrons in connection with cutoffs above and below the Fermi energy, as defined in Ref. [36]. Similar implementations of the angular-momentum-projected GCM have been developed also for the nonrelativistic Gogny interaction [37] and for relativistic mean-field Lagrangians [38].

To define a dimensionless deformation parameter, we use the sharp edge liquid drop relation between the axial quadrupole moment $Q_2^{(i)}$ and a parameter $\beta_2^{(i)}$:

$$\beta_2^{(i)} = \sqrt{\frac{5}{16\pi}}\frac{4\pi\, Q_2^{(i)}}{3R^2A}, \tag{1}$$

with $R = 1.2A^{1/3}$ fm. The mass dependence of the quadrupole moment is partly removed in this parameter β_2. It should not be compared with the multipole expansion parameters used in microscopic-macroscopic models, whose origin is not the same and usually are significantly smaller.

With our method, $B(E2, J \to J')$ values for in-band and out-of-band transitions as well as spectroscopic multipole moments $Q_s(J)$ are determined directly in the laboratory frame of reference [39]. As we use the full model space of occupied states, we do not have to distinguish between valence particles and a core, nor is there a need for effective charges.

To make a comparison with other approaches easier, it is useful to define quantities similar to intrinsic frame deformations from the spectroscopic and transition moments. An intrinsic transition charge quadrupole moment $Q^{(t)}$ can be derived from the $B(E2)$ values within the static rotor model:

$$Q^{(t)}(J) = \sqrt{\frac{16\pi}{5}\frac{B(E2, J \to J-2)}{(J0\,20|J-20)^2e^2}}. \tag{2}$$

In the same way, an intrinsic charge quadrupole moment can be related to the spectroscopic quadrupole moment $Q_c(J)$ via the relation

$$Q^{(s)}(J) = \frac{(J+1)(2J+3)}{3K^2 - J(J+1)}Q_c(J). \tag{3}$$

For axially symmetric shapes (i.e., pure $K = 0$ states), this relation reduces to $Q^{(s)}(J) = -Q_c(J)\,(2J+3)/J$, with a change of sign between $Q^{(s)}$ and $Q_c(J)$. Dimensionless deformation parameters $\beta_2^{(t)}$ and $\beta_2^{(s)}$ can be determined from $Q^{(t)}$ and $Q^{(s)}$, respectively, through an equation similar to Eq. (1), with A replaced by Z. Within a given band, $Q^{(s)}$ and $Q^{(t)}$ might still depend strongly on angular momentum.

$Q^{(s)}$ and $Q^{(t)}$ measure different properties: $Q^{(s)}$ depends on a single state, whereas $Q^{(t)}$ probes the geometry of the initial and final states whose wave functions can correspond to very different mixings of projected mean-field states. In general, these two moments take different values. Their near equality indicates that the assumptions of the static-rotor model are fulfilled; that is, there is a well-deformed rotational band not mixed with other bands.

III. RESULTS

A. Potential landscapes

Figure 1 provides the Nilsson diagram of the self-consistent single-particle energies for neutrons. The diagram for protons looks very similar, but shifted in energy. One can see two main differences with the single-particle energies used in some other methods. In the Woods-Saxon and the Folded-Yukawa potentials used in the microscopic-macroscopic calculations of Refs. [4] and [40], respectively, as in the Woods-Saxon potential used to generate the single-particle spectrum for the SMMC calculations of Ref. [12], the $p_{3/2}$ and $p_{1/2}$ levels are closer to the $g_{9/2}$ level by approximately 2 MeV and the separation between the $f_{5/2}$ and the $g_{9/2}$ levels is larger. As a result, the $p_{3/2}$ and the $f_{5/2}$ levels are much closer and their order is even changed in the case of the latter two models.

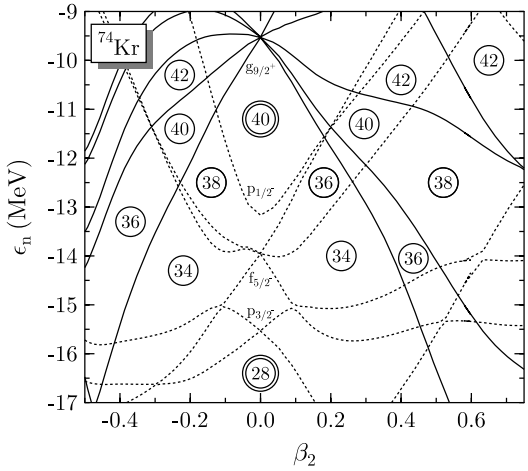

FIG. 1. Nilsson plot of neutron single-particle energies with positive (solid lines) and negative (dotted lines) parity as a function of the intrinsic mass deformation $\beta_2^{(i)}$, as obtained for ^{74}Kr.

These modifications have a strong effect on the deformed gaps, which may correspond to quite different deformations and vary in size. The spin-orbit splittings for the f and p levels in the three potentials are very similar to ours. The differences between the single-particle spectra must thus be related to the relative position of states with different orbital angular momentum within a given shell.

Figure 2 shows the mean-field and $J = 0$ projected energy curves for $^{72-78}$Kr obtained with the SLy6 Skyrme parametrization. Throughout this paper, the projected energy is plotted as a function of the intrinsic $\beta_2^{(i)}$ value of the mean-field states from which they are obtained. In our opinion, this quantity provides the most convenient and intuitive label that can be defined for all states, irrespective of the level of modeling. However, it should not be misinterpreted as an observable. With our method, one calculates transition and spectroscopic multipole moments in the laboratory frame, which can be directly compared to experimental data. However, the spectroscopic moments that characterize a state do not provide useful coordinates to plot potential energy curves because they scale with angular momentum and are even identically zero for $J = 0$. For projected states with $J > 0$ and large intrinsic deformation in nuclei with A larger than 100, $\beta_2^{(i)}$ is very close to the intrinsic deformation $\beta_2^{(s)}$ determined from the laboratory-frame quadrupole moment $Q^{(s)}$ through the static rotor model, Eq. (3). Note that any coordinate might be misleading for the GCM, as the metric is related to the inverse of the overlap matrix, which has no direct connection to any deformation.

The mean-field energy landscapes (dotted lines in Fig. 2) show that the energies of the four nuclei vary quite slowly with deformation. Our calculations also predict a transition from a nucleus with coexisting prolate and oblate minima in ^{72}Kr to a soft, spherical, anharmonic vibrator in ^{78}Kr. The many shallow local minima and plateaus in the total energy curves can be directly related to the gaps in the Nilsson diagram in Fig. 1.

The two minima in the mean-field energy curve (dotted line) of ^{74}Kr reflect the $N = 38$ gaps in the Nilsson diagram at small

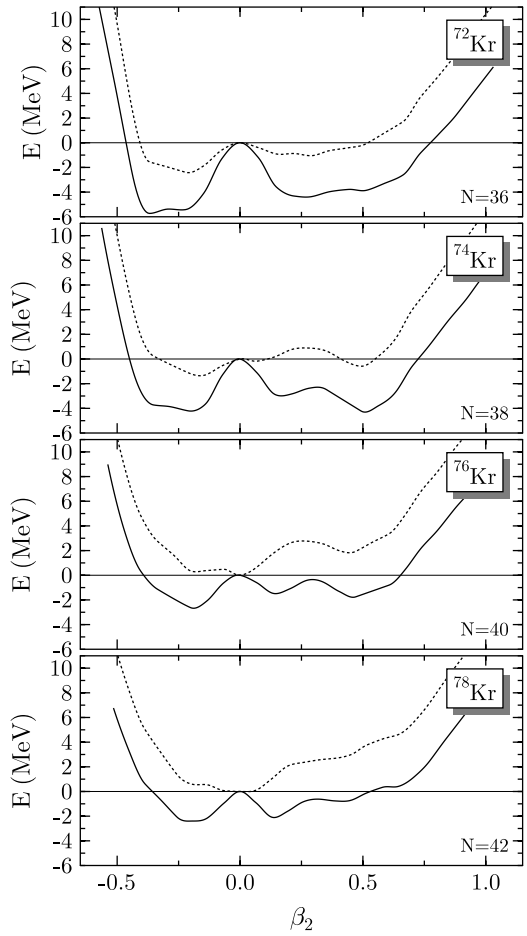

FIG. 2. Mean-field (dotted) and $J = 0$ projected deformation energy curves (solid) for $^{72-78}$Kr (see text).

oblate and large prolate deformations. For ^{76}Kr, the spherical mean-field minimum is related to the large spherical $N = 40$ subshell closure, whereas the shallow oblate and prolate structures correspond to two deformed $N = 40$ gaps in the Nilsson diagram. The prolate minimum has moved to smaller deformation than in ^{74}Kr, with the deformed $N = 38$ gap being at larger deformations than the $N = 40$ gap. The spherical $N = 40$ subshell closure is strong enough to stabilize the spherical shape up to the $N = 42$ isotope ^{78}Kr.

As can be seen from the solid lines in Fig. 2, the energy landscapes are qualitatively modified by the projection on $J = 0$. Since a spherical mean-field state is already a $J = 0$ state, the energy gain by projecting it on angular momentum is zero whereas the projection of a deformed mean-field state always leads to an energy gain, which increases very rapidly at small deformation. In almost all spherical and soft nuclei, this creates minima at prolate and oblate deformations with $|\beta_2^{(i)}|$ values around 0.1. These states usually have a large overlap close to 1, which means they are not two different states but represent the same one, which can be associated with a "correlated spherical state." In nuclei with shallow mean-field minima at small deformations as in the Kr isotopes, the projection merges this near-spherical spherical minimum with the slightly oblate one into a broad structure.

Because the prolate mean-field minimum is at larger deformation, two distinct structures appear on the prolate side in $^{74-78}$Kr, a "spherical" one at a β_2 value around 0.15 and a well-deformed one at a β_2 value around 0.5.

The topology of the ^{72}Kr energy surface on the oblate side can hardly be explained by a single, large oblate $N = 36$ gap in the Nilsson diagram. The mean field and $J = 0$ minima at large oblate deformations seem to result from a delicate balance of shell effects from $N = 34$ to $N = 40$, which reduce the level density around the Fermi surface sufficiently to create a shallow oblate minimum and a very soft energy surface. The shallow minimum on the prolate side can be associated with two close $N = 36$ gaps.

The fact that the structures in the potential landscapes can be easily associated with gaps in a Nilsson diagram is an attractive feature of our approach, which makes the connection with simpler models straightforward. This is an advantage compared to the interacting shell model, in which states are constructed as nonintuitive np-nh states in a spherical basis.

One may wonder whether it is meaningful to restrict the description of the light Kr isotopes to axial shapes. There have been a few explorations of the triaxial degree of freedom, which can help answer this question. Yamagami *et al.* [41] have calculated the potential landscape of ^{72}Kr along several shape degrees of freedom, including nonaxial octupole deformations, using the Skyrme SIII interaction. Their potential energy curve is similar to ours for purely quadrupole axial deformations. They found that the prolate and oblate energy minima are separated by a triaxial barrier of 500 keV and that the oblate shapes are soft with respect to nonaxial octupole deformations. Bonche *et al.* [5] have obtained rather large triaxial barriers for ^{74}Kr and ^{76}Kr, also using the SIII interaction. Let us also mention that Almehed and Walet [42] have self-consistently determined a collective path in ^{72}Kr for different values of the angular momentum in a small model space using a schematic interaction. For $J = 0$, they obtain a purely axial path that connects the oblate ground state and the prolate minimum. For $J = 2$, the path that they obtain does not cross the spherical configuration and makes a small excursion through triaxiality, as can be expected from the projected energy curves. From these studies of triaxiality, one can conclude that, in most models, the oblate and prolate minima found as a function of the axial quadrupole moment are true minima. The barrier between the minima in the γ degree of freedom may not be very high, but to restrict the model to axial symmetry can be expected to provide a valid first approximation.

B. Spectroscopy

We first focus on the three isotopes for which very complete sets of experimental data are available. This enables us to introduce our notation and all the ingredients necessary for a comparison between our results and the data. We will return to the more prospective case of ^{72}Kr at the end.

1. ^{74}Kr

In Fig. 3 are given the lowest projected GCM levels for $J = 0$ up to 8 together with the corresponding projected

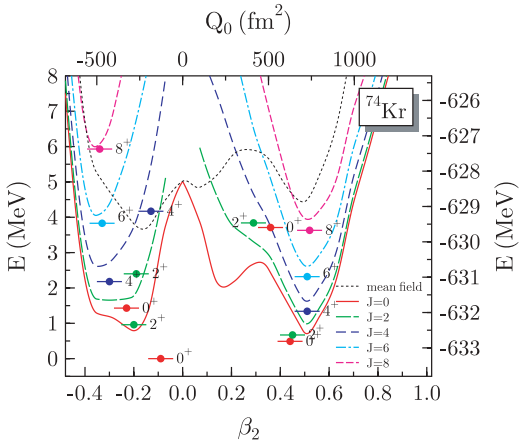

FIG. 3. (Color online) Mean-field energy curve, angular-momentum-projected energy curves, and projected GCM for ^{74}Kr. The projected energy curves are plotted as a function of the intrinsic deformation of the mean field from which they are projected; the projected GCM levels are plotted at the average deformation $\bar{\beta}_2$, Eq. (4). The labels on the right-hand side give the total binding energy as calculated; the labels on the left-hand side give the energy relative to the $J = 0$ GCM ground state.

energy curves. The collective levels are plotted at the mean deformation $\bar{\beta}_2^{(i)}$ of the mean-field states from which they are constructed, defined as

$$\bar{\beta}_2^{(i)} = \sum_{\beta_2^{(i)}} \beta_2^{(i)} \, g_{J,k}^2\big(\beta_2^{(i)}\big), \tag{4}$$

which provides in many cases an intuitive picture of the band structure in a nucleus. Figure 4, however, illustrates the limits of the meaning of $\bar{\beta}_2$, showing the collective wave functions g_i^J for $J = 0$, 2 and 4. All low-lying 0^+ states result from a strong mixing between prolate and oblate mean-field configurations. The values of $\bar{\beta}_2$ for the ground state and the second excited state reflect the dominance of oblate and prolate deformations. For the ground state 0^+, the very small value of $\bar{\beta}_2$ does not mean that this state is nearly spherical but, rather, that the weights of prolate and oblate shapes are nearly equal. For higher J values, the mixing between oblate and prolate configurations is less pronounced and the value of $\bar{\beta}_2$ better represents the structure of the states.

As can be seen in Fig. 2, the $J = 0$ projected energy curve for ^{74}Kr presents two nearly degenerate minima at oblate and large prolate deformations and a third shallow excited minimum at small deformation. This structure is reflected in the spectrum of GCM states plotted in Fig. 3 and in the wave functions drawn in Fig. 4.

As can be seen in Fig. 4, the $J = 0$ GCM wave functions strongly mix projected oblate, near-spherical, and prolate configurations. The near degeneracy of the oblate and prolate minima is lifted; the first excited 0^+ state has an excitation energy of 0.49 MeV. The situation becomes simpler for larger angular momenta. The first 2^+ level still strongly mixes prolate and oblate deformations and has a wave function rather similar to the first excited 0^+ state. In contrast, the second 2^+ state is mainly constructed from oblate mean-field configurations

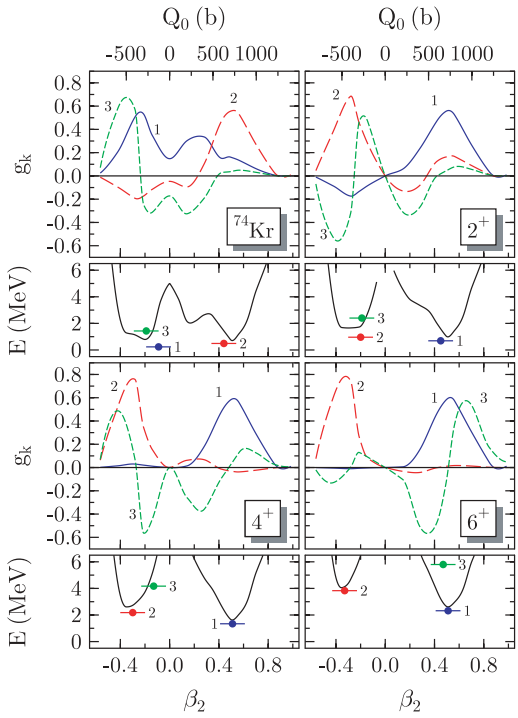

FIG. 4. (Color online) Collective wave functions $g_k^{(J)}$ for the lowest states with $J = 0$, 2, 4, and 6 for ^{74}Kr as a function of the intrinsic deformation of the mean-field states from which they are constructed. The corresponding energies and average deformations $\bar{\beta}_2$ are plotted together with the projected energy surface.

projected on $J = 2$ with a negative mean deformation larger in modulus than that of the ground state. The two first 4^+ and 6^+ states are dominated by only prolate or oblate deformations. One can thus expect that an approximation based on a fixed mean-field configuration, like the cranked mean-field methods, is justified beyond $J = 4$.

The nodal structure of the collective wave function is more complicated than the structure that one would obtain in a one-dimensional potential well. It reflects the fact that the rotation of a deformed wave function around the y axis generates wave functions that cannot be represented along a single axis: the exchange of the x and z axes generates prolate and oblate shapes for two different values of the angle γ. For this reason, the angular-momentum-projected GCM wave functions is not one dimensional, even when only axial states are mixed [39]. ^{74}Kr provides an excellent example that a comparison between the intrinsic deformation of a mean-field minimum and the transition quadrupole moment derived from a $B(E2)$ value might be misleading. There are three reasons for that: (i) For light and medium-mass nuclei, the minima of the projected energy curve are usually at larger prolate and oblate deformations than the minima of the mean-field energy curve, (ii) the minima of the projected $J = 0$ and $J = 2$ energy curves correspond to the projection of mean-field states with different deformation and the assumption of a static rotor is not valid at low angular momentum, and (iii) the wave functions of the low-lying states are quite broad and strongly mix oblate or prolate configurations; moreover, the mixing is different for the 0^+ states and 2^+ states.

A schematic two-level-mixing model has been used by Becker and co-workers [15,43] to analyze the experimental data. In this model, the energies of "pure" prolate and oblate configurations are deduced from an extrapolation to low spins of the high spin parts of the bands. This is valid if configuration mixing decreases with spin, which seems reasonable in view of our results. Data are described well by assuming that the unperturbed levels are nearly degenerate with only a 20-keV energy difference. This leads to nearly equal contributions from the oblate and prolate unperturbed states. This result is consistent with our calculations, although the assumption that one has to mix only two configurations is too crude. The complicated structures that we obtain for the collective wave functions, of Fig. 4 cannot be reduced to the mixing of two or even three configurations with a well-defined shape. It does not therefore seem possible to connect our results with a phenomenological two-level mixing model.

Theoretical and experimental excitation spectra and $B(E2)$ values are compared in Fig. 5. As in the experiment, the theoretical levels are ordered in bands on the basis of their spectroscopic quadrupole moments and of the dominant $E2$ transitions. A low-lying γ band, which has a 2^+ bandhead at 1.74 MeV, has been omitted since $K = 2$ states are outside our model space. The $B(E2)$ values are always given for transitions from $J \to J - 2$ or from $J \to J$, although values found in the literature correspond sometimes to $B(E2, J \to J + 2)$ values, which are by definition larger by a factor 5. Our calculation is only partly consistent with experiment. We reproduce the coexistence of oblate and prolate bands, strongly mixed at low angular momentum, but the lowest 0^+ states do not have the right ordering. Our calculated ground state is predominantly oblate, but the prolate band becomes yrast already at $J = 2$. For higher spins the spectrum is too stretched out, a problem that has already been encountered in previous GCM studies [34,35].

The in-band transition probabilities are slightly overestimated for both bands, which hints at a slightly too large

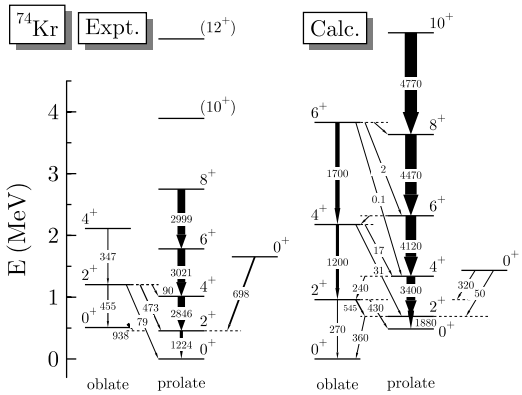

FIG. 5. Spectrum of collective states for ^{74}Kr as seen in experiment (left) and as obtained from our calculation (right). The arrows with numbers denote the $B(E2, J \to J - 2)$ values for transitions between states with different J and $B(E2, J \to J)$ for transitions between states with the same J, both given in e^2 fm^4. Experimental values for the $B(E2)$ values are taken from [24,25]. The labels "oblate" and "prolate" given to the bands correspond to the main components of the collective wave functions.

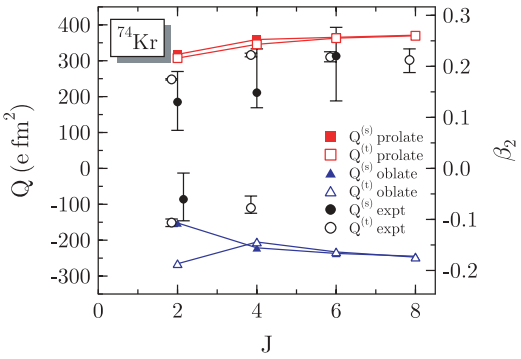

FIG. 6. (Color online) Comparison of calculated and experimental $Q^{(s)}(J)$ and $Q^{(t)}(J \to J-2)$ moments for states in the prolate and oblate bands, assuming that all states are purely axial. Note that $-Q^{(t)}$ is plotted for oblate states for better comparison with $Q^{(s)}$. Experimental values are taken from [25].

deformation of the dominating configurations in both bands. Nevertheless, all calculated values are within a factor of 2 of the experimental ones. Out-of-band transitions between states at the bottom of the bands are large, in particular the experimental value of $B(E2, 2^+_{\rm pro} \to 0^+_{\rm obl})$ of 938^{+110}_{-91} e^2 fm^4 given in [25] or 1120 ± 460 e^2 fm^4 given in [16] Our predicted out-of-band $B(E2)$ values become weak already at $J = 4$.

The theoretical spectroscopic quadrupole moments are compared with experiment in Fig. 6. These moments provide by their sign the only unambiguous way to assign a prolate or an oblate character to a band. To compare them with in-band $B(E2)$ values as well, $Q^{(s)}$ and $Q^{(t)}$ values derived from the static rotor model assuming $K = 0$ are shown. Except for the oblate 2^+ state, our calculated $Q^{(s)}$ and $Q^{(t)}$ values are very similar. Experimental values for $Q^{(s)}$ and $Q^{(t)}$ are also similar within the large error bars of $Q^{(s)}$. Our calculation gives systematically larger deformation for both the prolate and oblate states, as already discussed.

2. ^{76}Kr

The projected energy curves in ^{76}Kr, plotted in Fig. 7, are very similar to those obtained for ^{74}Kr, with coexisting

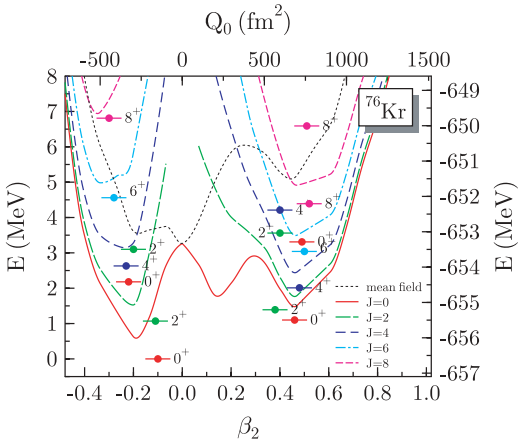

FIG. 7. (Color online) The same as Fig. 3 for ^{76}Kr.

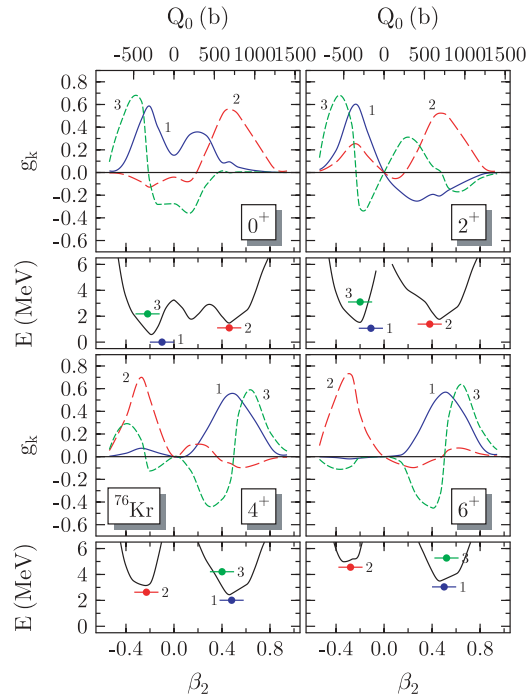

FIG. 8. (Color online) The same as Fig. 4, but for ^{76}Kr.

prolate and oblate bands, except that the prolate minima at β_2 values around 0.45 are less pronounced. As a consequence, the ground-state wave function is more dominated by oblate configurations than that of ^{74}Kr, as confirmed by the shape of the collective wave functions given in Fig. 8. This is at variance with experiment, which indicates a prolate ground state (see also Fig. 9). Again, we omit from Fig. 9 the experimental states assigned to a γ band with a 2^+ bandhead at 1.222 MeV (see, e.g. [21,25]). The calculated prolate bandhead has a higher excitation energy than that for ^{74}Kr. The prolate band becomes yrast at $J = 4$. Compared to ^{74}Kr, the increased "purity" of states within the prolate and oblate bands happens at higher angular momenta, which is reflected in the large out-of-band $B(E2)$ values up to $J = 4$ in Fig. 9.

Figure 10 compares the intrinsic quadrupole moments. As for ^{74}Kr, our calculated values for $Q^{(s)}$ and $Q^{(t)}$ are very

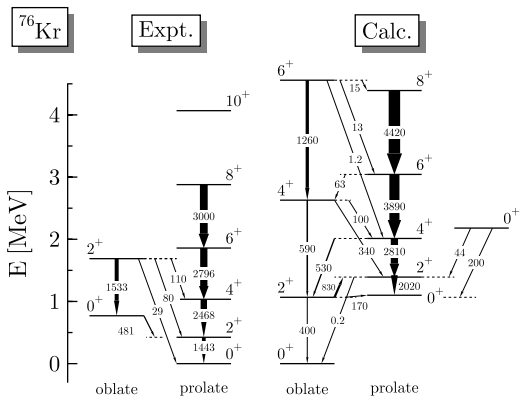

FIG. 9. The same as Fig. 5, but for ^{76}Kr. Experimental data are taken from Ref. [25].

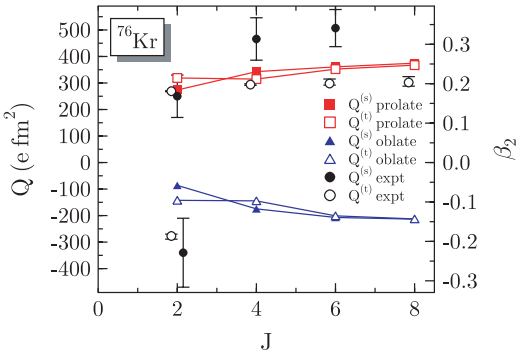

FIG. 10. (Color online) The same as Fig. 6, but for ^{76}Kr. Experimental values are taken from Ref. [25].

similar, with small deviations at low J. Notably, this is not the case for the experimental values when assuming $K = 0$, which might hint at a small admixture of triaxial shapes to the prolate band, which is outside the scope of our calculation. Our calculated $Q^{(t)}$ values are very close to the experimental values for the prolate band, whereas the $Q^{(t)}$ of the 2^+ state in the oblate band is underestimated.

3. ^{78}Kr

Among the Kr isotopes, ^{78}Kr has the lowest excitation energy for the first 2^+ state and the largest $B(E2, 2_1^+ \rightarrow 0_1^+)$ value, corresponding to a transition quadrupole deformation $\beta_2^{(t)}$ of 0.35. The rotational band built on the ground state has been seen up to $J = 24$. Two additional bands are known at low excitation energy, a first usually interpreted as a γ band built on a low-lying 2^+ state at 1.148 MeV and a second one built on a 0^+ state at 1.017 MeV, originally assumed to be oblate. According to the recent analysis of [26], the spectroscopic quadrupole moment of the 2^+ state in this band is negative, which indicates that this band should, in fact, be prolate.

Looking to the energy curves of ^{78}Kr, the collective states obtained from the projected GCM, Fig. 11, and the collective wave functions, Fig. 12, one can attribute to the ground state a dominating oblate structure and to the bandhead of the first

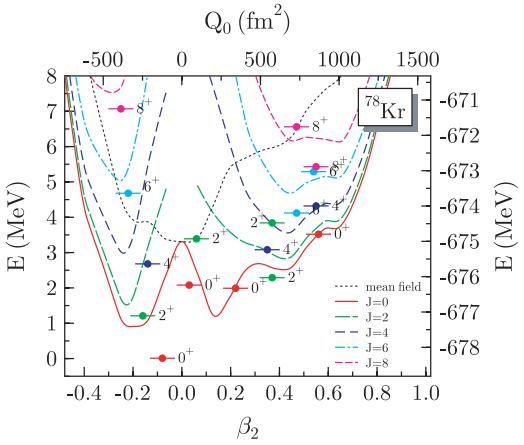

FIG. 11. (Color online) The same as Fig. 3, but for ^{78}Kr.

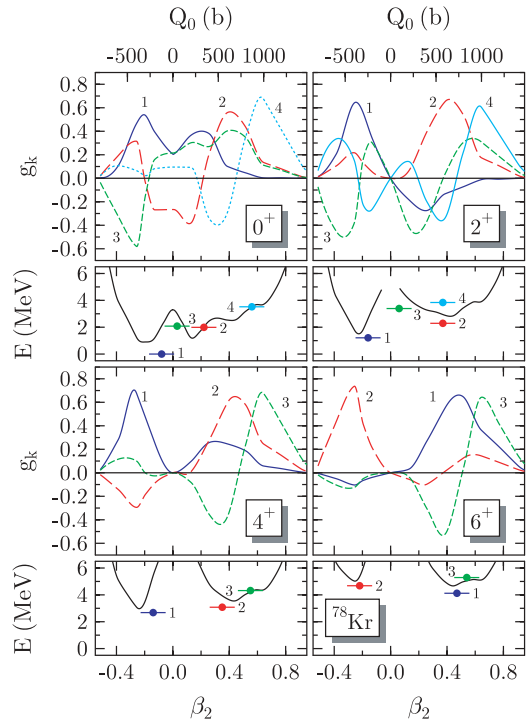

FIG. 12. (Color online) The same as Fig. 4, but for ^{78}Kr.

excited band, located at 2 MeV, a well-deformed prolate shape. All low-lying states are strongly mixed, which leads to large out-of-band $B(E2)$ values up to $J = 6$.

Data for transition moments are taken from a recent Coulomb excitation experiment [26]. Values for in-band transitions in the yrast band were published earlier in Refs. [20,27], with a $B(E2; 2_1^+ \rightarrow 0_2^+)$ value of 91(5) e^2 fm^4 in [17], compatible with the value of 130(40) e^2 fm^4 obtained in [26].

As can be seen in Figs. 13 and 14, our values are close to the experimental data for the low-lying states in the prolate band. The slight increase of $Q^{(t)}$ with J that we obtain can be related to the gradual disappearance of the prolate minimum at β_2 values around 0.45 and to the deepening of the shoulder at β_2 values around 0.6, which becomes the prolate minimum

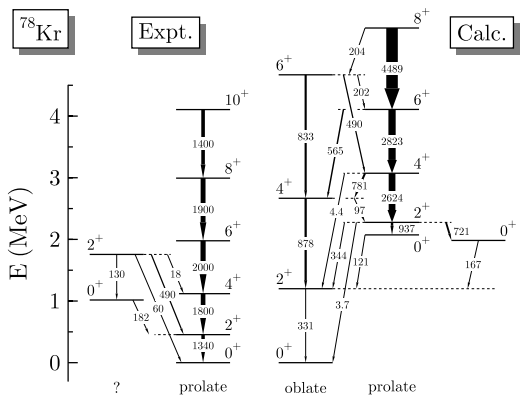

FIG. 13. The same as Fig. 5, but for ^{78}Kr. Experimental values for the $B(E2)$ values are taken from Ref. [26].

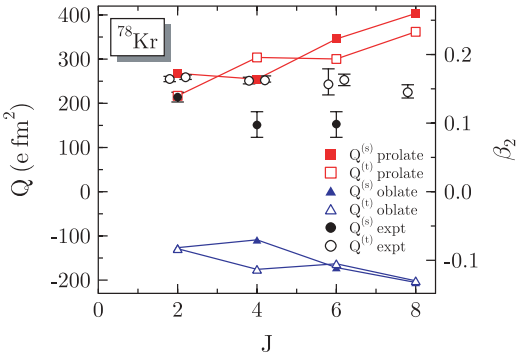

FIG. 14. (Color online) The same as Fig. 6, but for ^{78}Kr. Experimental values are taken from Refs. [20,26].

at $J \geqslant 8$ (see Fig. 11). In contrast, the experimental $Q^{(t)}$ values are constant or slightly decreasing with J, see also [20,27].

The large mixing between the prolate 0^+ state with another excited 0^+ state considerably reduces the in-band $B(E2; 2^+_{\rm pro} \to 0^+_{\rm pro})$ value, as the $E2$ strength from the $2^+_{\rm pro}$ level is nearly equally distributed. Therefore, our $B(E2; 2^+_{\rm pro} \to 0^+_{\rm pro})$ probability is slightly smaller than the experimental $B(E2; 2^+_1 \to 0^+_1)$ from the corresponding experimental state. As a consequence of this strong mixing, the calculated $Q^{(s)}$ and $Q^{(t)}$ values differ more than for ^{74}Kr and ^{76}Kr, with $Q^{(s)}$ being larger than $Q^{(t)}$ except for $J = 4$. Experimentally, $Q^{(s)}$ values are smaller than $Q^{(t)}$ ones [26].

4. ^{72}Kr

Rotational bands at high spin in ^{72}Kr have been investigated extensively, mainly motivated by the quest for fingerprints of $T = 0$ proton-neutron pairing [44,45]. Much less is known about the structure of this nucleus at low excitation energy. Only one band and two states that cannot be grouped into bands have been observed at low spin [16]. The precise structure of the low-spin yrast states is not completely clear either, as the ground state is argued to be oblate, in parts by consistency with theoretical predictions, whereas at higher spin the yrast states are assumed to be prolate. It was also argued in Ref. [18]

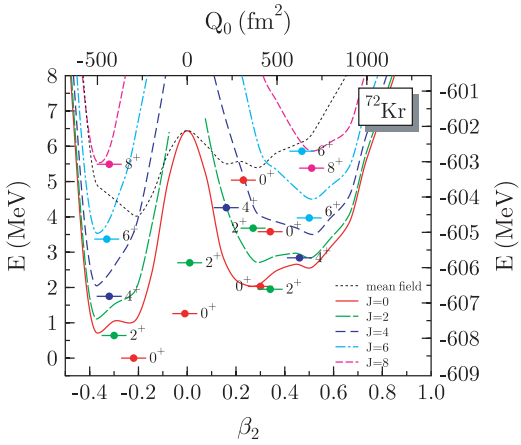

FIG. 15. (Color online) The same as Fig. 3, but for ^{72}Kr.

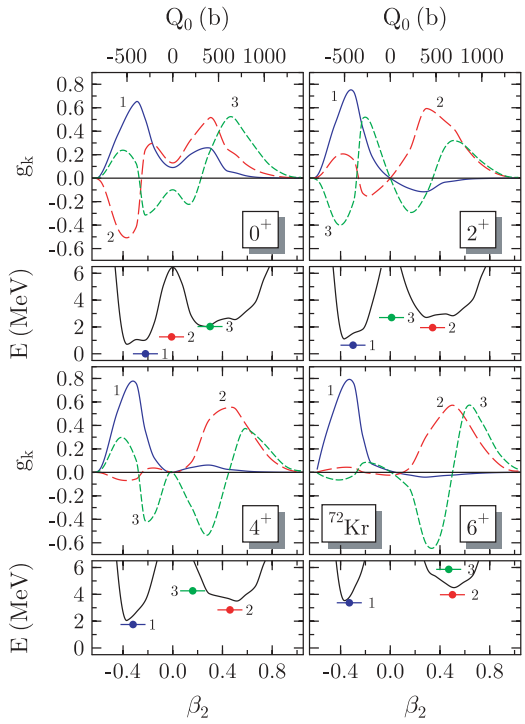

FIG. 16. (Color online) The same as Fig. 4, but for ^{72}Kr.

that the large $Q^{(t)}$ value obtained from the $B(E2; 8^+ \to 6^+) = 2090(780)\, e^2$ fm^4 values favors its interpretation as a transition between prolate states.[1] We obtain, however, a much larger $B(E2)$ for the $8^+_{\rm pro} \to 6^+_{\rm pro}$ transition than the experimental value, which is in fact consistent with our $8^+_{\rm obl} \to 6^+_{\rm obl}$ value. In view of the systematic overestimation of the experimental $B(E2)$'s at large spins given by our method for the heavier Kr isotopes, one cannot draw a conclusion on the nature of the 8^+ state in ^{72}Kr. However, it is clear that these large $B(E2)$ values do not exclude an oblate band as previously argued.

The potential energy curves, together with the GCM spectra, are shown in Fig. 15 and the collective wave functions in Fig. 16. According to the usual interpretation of the two low-lying 0^+ states, our calculation reproduces their order with a dominantly oblate ground state. In Fig. 17, the experimental and theoretical excitation energies and $B(E2)$ values are compared. According to the usual interpretation of the two low-lying 0^+ states, our calculation reproduces their order with a dominantly oblate ground state. The first excited 2^+ state is at about the same excitation energy as the experimental one, whereas the first excited 0^+ state is slightly too high. Our calculated oblate states are yrast up to $J = 6$. With the exception the low-lying 0^+ states, which strongly mix oblate, spherical, and prolate states, the mixing between the prolate and oblate configurations is less important than for the heavier Kr isotopes. Within the accuracy that can be expected from our model, our $B(E2)$ value for the $2^+_{\rm obl} \to 0^+_{\rm obl}$ transition is consistent with the experimental one,

[1]The authors of Ref. [18] use a definition of β_2 different from ours, so the values cannot and should not be compared.

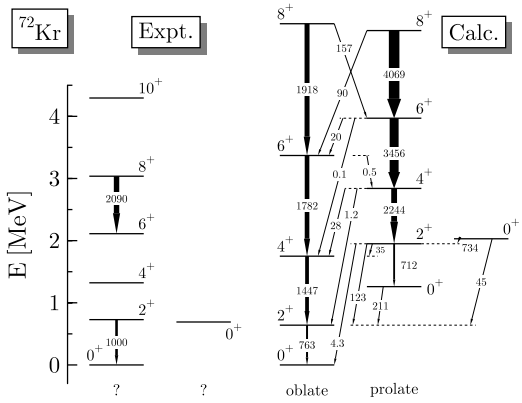

FIG. 17. The same as Fig. 5, but for ^{72}Kr. There is no unambiguous assignment of the experimental yrast states into a prolate or oblate band (see text). Experimental data for the $B(E2)$ values are taken from [18] ($8^+ \rightarrow 6^+$) and [22] ($2_1^+ \rightarrow 0_1^+$).

$B(E2; 2_1^+ \rightarrow 0_1^+) = 1000(130)\ e^2\ \mathrm{fm}^4$. ^{72}Kr is the only Kr isotope studied here for which we can assume to reproduce the ordering of the low-lying states.

C. $E0$ transitions and radii

The nuclear matrix element entering the monopole decay rate of a J^π state to a state with the same spin and parity is given by [46]

$$\rho^2_{E0}(J_{k'} \rightarrow J_k) = \left| \frac{\langle JMk|\hat{r}^2|JMk'\rangle}{R^2} \right|^2, \qquad (5)$$

where $R = 1.2A^1/3$ fm. Within a simple model [47], this matrix element can be related to the amount of mixing of configurations with different deformations in the physical states. As it is a nondiagonal matrix element, it is also very sensitive to the detailed structure of the initial and final states. Within the error bars, the experimental ρ^2_{E0} values are very close for $^{72-76}$Kr and slightly smaller for ^{78}Kr. The variation of the GCM values is much larger, but in view of their sensitivity to model details it is encouraging that our calculated ρ^2_{E0} values are within the experimental error bars for ^{74}Kr and ^{78}Kr and underestimate the value for ^{72}Kr by only a factor of 2. The large underestimation for ^{76}Kr can be related to the much smaller mixing between the oblate and prolate 0^+ states that we obtain for this isotope.

The reasonable description of the ρ^2_{E0} states indicates that, with the exception of ^{76}Kr, we have about the right amount of mixing between the oblate and prolate 0^+ states, which is independent of the relative placement of the energy levels. In contrast, the systematics of ground-state radii is not well described, as our calculations give the "wrong" ground state for $^{74-78}$Kr. This can be seen from the right panel of Fig. 18, where the isotopic shifts of the mean-square charge radii,

$$\delta r^2(N) = r^2(N) - r^2(N = 50), \qquad (6)$$

are plotted. The Kr radii present an anomaly [48,49]: they are larger for $^{74-84}$Kr than for the $N = 50$ isotope ^{86}Kr. The standard interpretation is that the ground states have an increasing

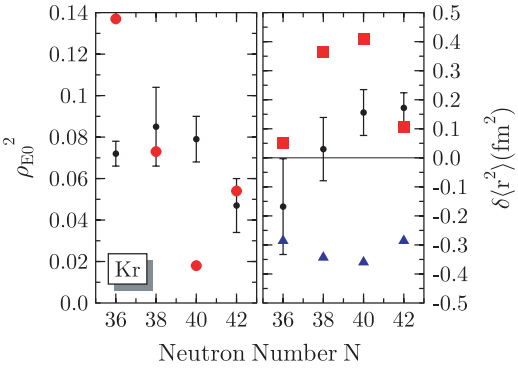

FIG. 18. (Color online) Left panel: Comparison of calculated values for $\rho^2_{E0}(0_2^+ \rightarrow 0_1^+)$ with experiment. Experimental values are taken from [16] ($^{72-74}$Kr) and [17] ($^{76-78}$Kr). Right panel: Isotopic shift of the mean-square charge radii for the lowest (dominantly) oblate 0^+ state (triangles) and the lowest (dominantly) prolate 0^+ state (squares). The ground state predicted by our calculation is always oblate.

admixture of prolate states of large deformation when going to more neutron-deficient nuclei, which overcompensates the volume effect of decreasing mass. Because our calculations always predict dominantly oblate ground states, we obtain a negative isotopic shift for all isotopes (triangles in the right panel of Fig. 18). Our calculated excited dominantly prolate 0^+ states, by contrast, lead to positive isotopic shifts for all four isotopes. It is unclear how well the ground state of ^{86}Kr itself is described within our method, so one has to be careful with the interpretation of the absolute values of the isotopic shifts. However, the δr^2 data confirm once again that the prolate states should have a much larger contribution to the ground state.

The relativistic mean-field calculations with the NL-SH interaction presented in Ref. [7] do reproduce the systematics of the isotopic shifts, which hints at the more realistic single-particle spectrum of this interaction in the *fp* shell.

IV. DISCUSSION AND CONCLUSIONS

Our results show that in medium-mass nuclei with coexisting shallow minima in soft potential energy landscapes, one has to be very cautious when comparing experimental data and the mean-field states corresponding to local minima. Projection on good angular momentum significantly alters the potential energy surfaces. After configuration mixing, the collective wave functions present a very large spreading and may extend over several mean-field minima. We also find rotational bands, for example in ^{78}Kr, that, rather then being related to a minimum in the mean-field energy landscape, are related to a plateau.

Although our calculations reproduce many of the global features of the neutron-deficient Kr isotopes, in closer detail there remain a couple of discrepancies with experiment.

(i) The collective spectra are too spread out in excitation energy, which appears to be a general problem of GCM of angular-momentum-projected axial mean-field states [34,35]. This problem could probably be cured by a larger

variational space for the projected GCM, in particular by treating dynamically the pairing, by breaking axial symmetry or time-reversal invariance. Breaking axial symmetry will also permit the description of γ bands. Work in these various directions is underway.

(ii) Our study of neutron-deficient Kr isotopes clearly points at a problem with the SLy effective interactions in the *fp* shell, related to the relative position of a few single-particle levels.

As already discussed in the literature, (see, e.g., the discussion in [12]), the spectroscopic properties of the neutron-deficient Kr region are extremely sensitive to the details of the shell structure. The number of levels around the Fermi energy is quite small, which results in several shell gaps for every neutron and proton number from 34 to 42. Any change in the relative position of levels and of their ordering will modify the size and deformation of the gaps in Fig. 1.

Our results, and those of models with adjustable single-particle spectra that perform better for Kr isotopes, suggest a few necessary modifications of the single-particle spectra obtained with the SLy6 Skyrme parametrization:

(i) The experimental evidence that there are no spherical 0^+ states in the spectrum of ^{76}Kr shows that the $N = 40$ spherical shell gap is too strong. This is consistent with our results for the $N \approx Z \approx 40$ region obtained in a systematic study of mass and deformation where the obtanined ground state for ^{80}Zr was spherical with a very pronounced shell effect [50], whereas experiment suggests that it is a well-deformed rotor [51]. A $g_{9/2}$ level closer to the $p_{1/2}$ orbital would decrease the $N = 40$ spherical gap It would also decrease the oblate $N = 38$ gap, and shift the prolate $N = 38$ gap to smaller deformation, probably reducing the deformation of ^{74}Kr.

(ii) If we take the Woods Saxon single-particle level schemes of Fig. 17 in [40] as an example, a decrease of the separation between the $f_{5/2}$ and the $p_{3/2}$ levels should change the single-particle spectra at small prolate deformation: a gap at $N = 38$ that extends from oblate shapes to prolate shapes would replace the gap at $N = 36$ around $\beta_2 = 0.2$. It can be expected that this would drive ^{74}Kr toward prolate shapes.

We have checked that all modern successful Skyrme interactions give single-particle spectra in the *fp* shell that are similar to those obtained with SLy6. This points to a deficiency of the standard Skyrme interaction in general and not to a difficulty intrinsic to SLy6. Other models such as the relativistic mean-field (RMF) model might seem to work more satisfactorily in the *fp* shell and to predict potential landscapes in better qualitative agreement with the Kr data than ours [7]. However, those models do not describe correctly the neutron-deficient Pb region [52,53], where many Skyrme forces perform quite well [30,31].

Altogether, the present study confirms the conclusions drawn in [50] that the current functional form of the Skyrme energy functional is not yet flexible enough to cover the relevant aspects of nuclear structure with the same good quality for all regions of the nuclear chart.

The combined analysis of Figs. 1 and 2 suggests that the structure of collective states in the neutron-deficient krypton isotopes provides a sensitive testing ground for future attempts to construct better effective interactions. It has been pointed out recently that a tensor interaction, absent in the existing standard mean-field models, introduces a particle-number dependence of single-particle spectra [54–56]; this might resolve at least some of the deficiencies in the *fp* shell that we encounter here and that are known for other regions of the nuclear chart. Work in that direction is underway.

ACKNOWLEDGMENTS

Work by M.B. was performed within the framework of L'Espace de Structure Nucléaire Théorique (ESNT). We thank E. Bouchez, E. Clément, A. Gade, A. Görgen, and W. Korten for stimulating discussions on the available experimental data and for making their results available to us prior to publication. We also thank R. V. F. Janssens and C. J. Lister for interesting discussions. This work was supported by the Belgian Science Policy Office under Contract No. PAI P5-07 and the U.S. National Science Foundation under Grant No. PHY-0456903. MB acknowledges financial support from the European Commission. MB and PHH are grátéful for the hospitality at the Institute for Nuclear Theory, Seattle, where part of this work was carried out.

[1] M. Bender, P.-H. Heenen, and P.-G. Reinhard, Rev. Mod. Phys. **75**, 121 (2003).
[2] J. L. Wood, K. Heyde, W. Nazarewicz, M. Huyse, and P. van Duppen, Phys. Rep. **215**, 101 (1992).
[3] F. Dickmann, V. Metag, and R. Repnow, Phys. Lett. **38B**, 207 (1972).
[4] W. Nazarewicz, J. Dudek, R. Bengtsson, and I. Ragnarsson, Nucl. Phys. **A435**, 397 (1985).
[5] P. Bonche, H. Flocard, P.-H. Heenen, S. J. Krieger, and M. S. Weiss, Nucl. Phys. **A443**, 39 (1985).
[6] M. Girod, J. P. Delaroche, D. Gogny, and J. F. Berger, Phys. Rev. Lett. **62**, 2452 (1989).
[7] G. A. Lalazissis and M. M. Sharma, Nucl. Phys. **A586**, 201 (1995).
[8] U. Kaup and A. Gelberg, Z. Phys. A **311**, 293 (1979).
[9] A. Petrovici, A. Faessler, and Th. Koppel, Z. Phys. A **314**, 227 (1983).
[10] A. Petrovici, K. W. Schmid, and A. Faessler, Nucl. Phys. **A665**, 333 (2000).
[11] A. Petrovici, K. W. Schmid, and A. Faessler, Nucl. Phys. **A708**, 190 (2002).
[12] K. Langanke, D. J. Dean, and W. Nazarewicz, Nucl. Phys. **A728**, 109 (2003).
[13] R. B. Piercey, J. H. Hamilton, R. Soundranayagam, A. V. Ramayya, C. F. Maguire, X.-J. Sun, Z. Z. Zhao, R. L. Robinson, H. J. Kim, S. Frauendorf, J. Döring, L. Funke, G. Winter, J. Roth, L. Cleemann, J. Eberth, W. Neumann, J. C. Wells, J. Lin, A. C. Rester, and H. K. Carter, Phys. Rev. Lett. **47**, 1514 (1981).

[14] C. Chandler, P. H. Regan, C. J. Pearson, B. Blank, A. M. Bruce, W. N. Catford, N. Curtis, S. Czajkowski, W. Gelletly, R. Grzywacz, Z. Janas, M. Lewitowicz, C. Marchand, N. A. Orr, R. D. Page, A. Petrovici, A. T. Reed, M. G. Saint-Laurent, S. M. Vincent, R. Wadsworth, D. D. Warner, and J. S. Winfield, Phys. Rev. C **56**, R2924 (1997).

[15] F. Becker, W. Korten, F. Hannachi, P. Paris, N. Buforn, C. Chandler, M. Houry, H. Hübel, A. Jansen, Y. Le Coz, C. F. Liang, A. Lopez-Martens, R. Lucas, E. Mergel, P. H Regan, G. Schönwasser, and C. Theisen, Eur. Phys. J. A **4**, 103 (1999).

[16] E. Bouchez, I. Matea, W. Korten, F. Becker, B. Blank, C. Borcea, A. Buta, A. Emsallem, G. de France, J. Genevey, F. Hannachi, K. Hauschild, A. Hürstel, Y. Le Coz, M. Lewitowicz, R. Lucas, F. Negoita, F. de Oliveira Santos, D. Pantelica, J. Pinston, P. Rahkila, M. Rejmund, M. Stanoiu, and Ch. Theisen, Phys. Rev. Lett. **90**, 082502 (2003).

[17] A. Giannatiempo, A. Nannini, A. Perego, P. Sona, M. J. G. Borge, O. Tengblad, and the ISOLDE Collaboration, Phys. Rev. C **52**, 2444 (1995).

[18] G. de Angelis, C. Fahlander, A. Gadea, E. Farnea, W. Gelletly, A. Aprahamian, D. Bazzacco, F. Becker, P. G. Bizzeti, A. Bizzeti-Sona, F. Brandolini, D. de Acuna, M. De Poli, J. Eberth, D. Foltescu, S. M. Lenzi, S. Lunardi, T. Martinez, D. R. Napoli, P. Pavan, C. M. Petrache, C. Rossi Alvarez, D. Rudolph, B. Rubio, W. Satuła, S. Skoda, P. Spolaore, H. G. Thomas, C. A. Ur, and R. Wyss, Phys. Lett. **B415**, 217 (1997).

[19] A. Algora, G. de Angelis, F. Brandolini, R. Wyss, A. Gadea, E. Farnea, W. Gelletly, S. Lunardi, D. Bazzacco, C. Fahlander, A. Aprahamian, F. Becker, P. G. Bizzeti, A. Bizzeti-Sona, D. de Acuña, M. De Poli, J. Eberth, D. Foltescu, S. M. Lenzi, T. Martinez, D. R. Napoli, P. Pavan, C. M. Petrache, C. Rossi Alvarez, D. Rudolph, B. Rubio, S. Skoda, P. Spolaore, R. Menegazzo, H. G. Thomas, and C. A. Ur, Phys. Rev. C **61**, 031303(R) (2000).

[20] P. K. Joshi, H. C. Jain, R. Palit, G. Mukherjee, and S. Nagaraj, Nucl. Phys. **A700**, 59 (2002).

[21] J. J. Valiente-Dobón, C. E. Svensson, C. D. O'Leary, I. Ragnarsson, C. Andreoiu, D. E. Appelbe, R. A. E. Austin, G. C. Ball, J. A. Cameron, M. P. Carpenter, R. M. Clark, M. Cromaz, D. Dashdorj, P. Fallon, P. Finlay, S. J. Freeman, P. E. Garrett, A. Görgen, G. F. Grinyer, D. F. Hodgson, B. Hyland, D. Jenkins, F. Johnston-Theasby, P. Joshi, N. S. Kelsall, A. O. Macchiavelli, F. Moore, G. Mukherjee, A. A. Phillips, W. Reviol, D. Sarantites, M. A. Schumaker, D. Seweryniak, M. B. Smith, J. C. Waddington, R. Wadsworth, D. Ward, and S. J. Williams, Phys. Rev. C **71**, 034311 (2005).

[22] A. Gade, D. Bazin, A. Becerril, C. M. Campbell, J. M. Cook, D. J. Dean, D.-C. Dinca, T. Glasmacher, G. W. Hitt, M. E. Howard, W. F. Mueller, H. Olliver, J. R. Terry, and K. Yoneda, Phys. Rev. Lett. **95**, 022502 (2005).

[23] J. J. Valiente-Dobón, T. Steinhardt, C. E. Svensson, A. V. Afanasjev, I. Ragnarsson, C. Andreoiu, R. A. E. Austin, M. P. Carpenter, D. Dashdorj, G. de Angelis, F. Dönau, J. Eberth, E. Farnea, S. J. Freeman, A. Gadea, P. E. Garrett, A. Görgen, G. F. Grinyer, B. Hyland, D. Jenkins, F. Johnston-Theasby, P. Joshi, A. Jungclaus, K. P. Lieb, A. O. Macchiavelli, E. F. Moore, G. Mukherjee, D. R. Napoli, A. A. Phillips, C. Plettner, W. Reviol, D. Sarantites, H. Schnare, M. A. Schumaker, R. Schwengner, D. Seweryniak, M. B. Smith, I. Stefanescu, O. Thelen, and R. Wadsworth, Phys. Rev. Lett. **95**, 232501 (2005).

[24] A. Görgen, E. Clément, A. Chatillon, A. Dewald, W. Korten, Y. Le Coz, N. Marginean, B. Melon, R. Menegazzo, O. Möller, Ch. Theisen, D. Tonev, C. A. Ur, and K. O. Zell, Eur. Phys. J. A **26**, 153 (2005).

[25] E. Clément, A. Görgen, W. Korten, E. Bouchez, A. Chatillon, A. Hürstel, Y. Le Coz, Ch. Theisen, J. N. Wilson, C. Andreoui, F. Becker, P. Butler, J. M. Casandjian, W. N. Catford, T. Czosnyka, G. de France, J. Gerl, R.-D. Herzberg, J. Iwanicki, D. G. Jenkins, G. D. Jones, P. J. Napiorkowski, G. Sletten, C. Timis, and M. Zielinska (in preparation).

[26] F. Becker, A. Petrovici, J. Iwanicki, N. Amzal, W. Korten, K. Hauschild, A. Hurstel, Ch. Theisen, P. A. Butler, R. A. Cunningham, T. Czosnyka, G. de France, J. Gerl, P. Greenlees, K. Helariutta, R.-D. Herzberg, P. Jones, R. Julin, S. Juutinen, H. Kankaanpää, M. Muikku, P. Nieminen, O. Radu, P. Rahkila, and Ch. Schlegel, Nucl. Phys. **A770**, 107 (2006).

[27] A. Dhal, R. K. Sinha, P. Agarwal, S. Kumar, Monika, B. B. Singh, R. Kumar, P. Bringel, A. Neusser, R. Kumar, K. S. Golda, R. P. Singh, S. Muralithar, N. Madhavan, J. J. Das, A. Shukla, P. K. Raina, K. S. Thind, A. K. Sinha, I. M. Govil, P. K. Joshi, R. K. Bhowmik, A. K. Jain, S. C. Pancholi, and L. Chaturvedi, Eur. Phys. J. A **27**, 33 (2006).

[28] P. Bonche, J. Dobaczewski, H. Flocard, and P.-H. Heenen, Nucl. Phys. **A530**, 149 (1991).

[29] P.-H. Heenen, P. Bonche, J. Dobaczewski, and H. Flocard, Nucl. Phys. **A561**, 367 (1993).

[30] T. Duguet, M. Bender, P. Bonche, and P.-H. Heenen, Phys. Lett. **B559**, 201 (2003).

[31] M. Bender, P. Bonche, T. Duguet, and P.-H. Heenen, Phys. Rev. C **69**, 064303 (2004).

[32] P. Bonche, H. Flocard, and P.-H. Heenen, Comput. Phys. Commun. **171**, 49 (2005).

[33] D. L. Hill and J. A. Wheeler, Phys. Rev. **89**, 1102 (1953); J. J. Griffin and J. A. Wheeler, *ibid*. **108**, 311 (1957).

[34] M. Bender and P.-H. Heenen, Eur. Phys. J. A **25**, s01, 519 (2005).

[35] E. Chabanat, P. Bonche, P. Haensel, J. Meyer, and R. Schaeffer, Nucl. Phys. **A635**, 231 (1998); **A643**, 441(E) (1998).

[36] C. Rigollet, P. Bonche, H. Flocard, and P.-H. Heenen, Phys. Rev. C **59**, 3120 (1999).

[37] J. L. Egido and L. M. Robledo, in *Extended Density Functionals in Nuclear Physics*, edited by G. A. Lalazissis, P. Ring, and D. Vretenar, Lecture Notes in Physics No. 641 (Springer-Verlag, Berlin, 2004), p. 269.

[38] T. Niksic, D. Vretenar, and P. Ring, Phys. Rev. C **73**, 034308 (2006).

[39] M. Bender, H. Flocard, and P.-H. Heenen, Phys. Rev. C **68**, 044321 (2003).

[40] P. Möller, J. R. Nix, and K.-L. Kratz, At. Data Nucl. Data Tables **66**, 131 (1997).

[41] M. Yamagami, K. Matsuyanagi, and M. Matsuo, Nucl. Phys. **A693**, 579 (2001).

[42] D. Almehed and N. R. Walet, Phys. Lett. **B604**, 163 (2004).

[43] W. Korten, Acta Phys. Pol. B **32**, 729 (2001).

[44] S. M. Fischer, C. J. Lister, D. P. Balamuth, R. Bauer, J. A. Becker, L. A. Bernstein, M. P. Carpenter, J. Durell, N. Fotiades, S. J. Freeman, P. E. Garrett, P. A. Hausladen, R. V. F. Janssens, D. Jenkins, M. Leddy, J. Ressler, J. Schwartz, D. Svelnys, D. G. Sarantites, D. Seweryniak, B. J. Varley, and R. Wyss, Phys. Rev. Lett. **87**, 132501 (2001).

[45] S. M. Fischer, C. J. Lister, and D. P. Balamuth, Phys. Rev. C **67**, 064318 (2003).
[46] E. L. Church and J. Weneser, Phys. Rev. **103**, 1035 (1956).
[47] K. Heyde and R. A. Meyer, Phys. Rev. C **37**, 2170 (1988).
[48] M. Keim, E. Arnold, W. Borchers, U. Georg, A. Klein, R. Neugart, L. Vermeeren, R. E. Silverans, and P. Lievens, Nucl. Phys. **A586**, 219 (1995).
[49] P. Lievens, E. Arnold, W. Borchers, U. Georg, M. Keim, A. Klein, R. Neugart, L. Vermeeren, and R. E. Silverans, Europhys. Lett. **33**, 11 (1996).
[50] M. Bender, G. F. Bertsch, and P.-H. Heenen, Phys. Rev. C **73**, 034322 (2006).
[51] C. J. Lister, M. Campbell, A. A. Chishti, W. Gelletly, L. Goettig, R. Moscrop, B. J. Varley, A. N. James, T. Morrison, H. G. Price, J. Simpson, K. Connel, and O. Skeppstedt, Phys. Rev. Lett. **59**, 1270 (1987).
[52] K. Heyde, C. De Coster, P. Van Duppen, M. Huyse, J. L. Wood, and W. Nazarewicz, Phys. Rev. C **53**, 1035 (1996).
[53] T. Niksic, D. Vretenar, P. Ring, and G. A. Lalazissis, Phys. Rev. C **65**, 054320 (2002).
[54] T. Otsuka, presentation at the workshop on "Récents développements sur le champ moyen et l'appariément," Dapnia/SPhN, CEA Saclay, France, 28 June–8 July 2005.
[55] D. Brink, seminar at the IPN Orsay, France, March 2006.
[56] J. Dobaczewski, talk at the 3rd ANL/MSU/INT/JINA RIA Theory Workshop, Argonne, Illinois, 4–7 April 2006; nucl-th0604043.